

Dark Supergiant: *Chandra's* Limits on X-rays from Betelgeuse

Jennifer Posson-Brown, Vinay L. Kashyap, Deron O. Pease, and Jeremy J. Drake

*Smithsonian Astrophysical Observatory
60 Garden Street, MS-21
Cambridge, MA 02138*

jpbrown@head.cfa.harvard.edu

vkashyap@cfa.harvard.edu

dpease@cfa.harvard.edu

jdrake@cfa.harvard.edu

ABSTRACT

We have analyzed *Chandra* calibration observations of Betelgeuse (α Ori, M2 Iab, $m_V = 0.58$, 131 pc) obtained at the aimpoint locations of the HRC-I (8 ks), HRC-S (8 ks), and ACIS-I (5 ks). Betelgeuse is undetected in all the individual observations as well as cumulatively. We derive upper limits to the X-ray count rates and compute the corresponding X-ray flux and luminosity upper limits for coronal plasma that may potentially exist in the atmosphere of Betelgeuse over a range of temperatures, $T = 0.3 - 10$ MK. We place a flux limit at the telescope of $f_X \approx 4 \times 10^{-15}$ ergs s^{-1} cm^{-2} at $T = 1$ MK. The upper limit is lowered by a factor of ≈ 3 at higher temperatures, roughly an order of magnitude lower than that obtained previously. Assuming that the entire stellar surface is active, these fluxes correspond to a surface flux limit that ranges from $30 - 7000$ ergs s^{-1} cm^{-2} at $T = 1$ MK, to ≈ 1 ergs s^{-1} cm^{-2} at higher temperatures, five orders of magnitude below the quiet Sun X-ray surface flux. We discuss the implications of our analysis in the context of models of a buried corona and a pervasive magnetic carpet. We rule out the existence of a solar-like corona on Betelgeuse, but cannot rule out the presence of low-level emission on the scale of coronal holes.

Subject headings: stars: individual (Betelgeuse, α Ori) — stars: Mlab — X-rays: stars

1. Introduction

Betelgeuse (see Table 1) is a nearby (131 pc), bright ($V = 0.58^m$) evolved red supergiant star (M2 Iab, $B - V = 1.77$). It has been monitored extensively in the optical (e.g., Wilson et al. 1997, Burns et al. 1997), and displays irregular brightness variations ($V = 0.3 - 0.8$, Gray 2000) that have been interpreted as large-scale surface structures or activity (e.g., Lim et al. 1998 and Gray 2000). A definitive estimate of its age does not exist since it cannot be identified with nearby Orion associations (Lesh 1968), and estimates of its mass vary from $5 M_{\odot}$ (Dorch 2004) to $10 - 30 M_{\odot}$ (Gray 2000; also Lambert et al. 1984 and references therein). However, reasonable estimates can be obtained by comparing the evolutionary tracks of high-mass stars with the location of Betelgeuse on a color-magnitude diagram. We show such a comparison using the Geneva stellar evolutionary tracks (Lejeune & Schaerer 2001) in Figure 1. The stellar models vary in initial mass, metallicity, and mass-loss rates, and no rotation effects are included. While the systematic model uncertainties prevent a definitive assessment of the evolutionary history of Betelgeuse, note nevertheless that most of the models predict similar values of age and mass for the star, and therefore an approximate estimate of the gross properties of Betelgeuse is possible. Based on Figure 1, we adopt a current mass of $\approx 14 M_{\odot}$ and an age of ≈ 10 Myr for Betelgeuse. The uncertainty in these parameters do not affect our conclusions.

Betelgeuse has never been detected in X-rays, and is in a region of the H-R diagram where a stable corona is not expected to exist (Ayres et al. 1981, Linsky & Haisch 1979, Haisch, Schmitt, & Rosso 1991, Rosner et al. 1995, Hünsch & Schröder 1996, Hünsch et al. 1998). Nevertheless, there is evidence from numerical MHD simulations that dynamo action which can produce large scale magnetic fields can exist on such stars (Dorch 2004). Furthermore, chromospheric activity suggesting the presence of coronae has been detected in numerous late-type giant stars: coronal proxy lines such as Si IV and C IV have been detected in ostensibly non-coronal giants such as Arcturus and Aldebaran (Ayres et al. 2003); and forbidden coronal lines have been reported in *FUSE* observations of β Cet by Redfield et al. (2003). Thus, while unlikely, it is plausible that hot coronal plasma may exist on supergiants like Betelgeuse.

Here we present an analysis of X-ray observations of Betelgeuse obtained as part of the science instrument calibration program of the *Chandra* X-Ray Observatory (*Chandra*). The data are described in §2. Betelgeuse is not detected in X-rays in any of our individual observations or in co-added data, and in §3 we set the most stringent upper limits to the X-ray flux determined thus far, improving upon limits obtained from the *ROSAT* All-Sky Survey (RASS) by two orders of magnitude. In §4, we discuss our results in the context of models of coronae on late-type stars. We summarize in §5.

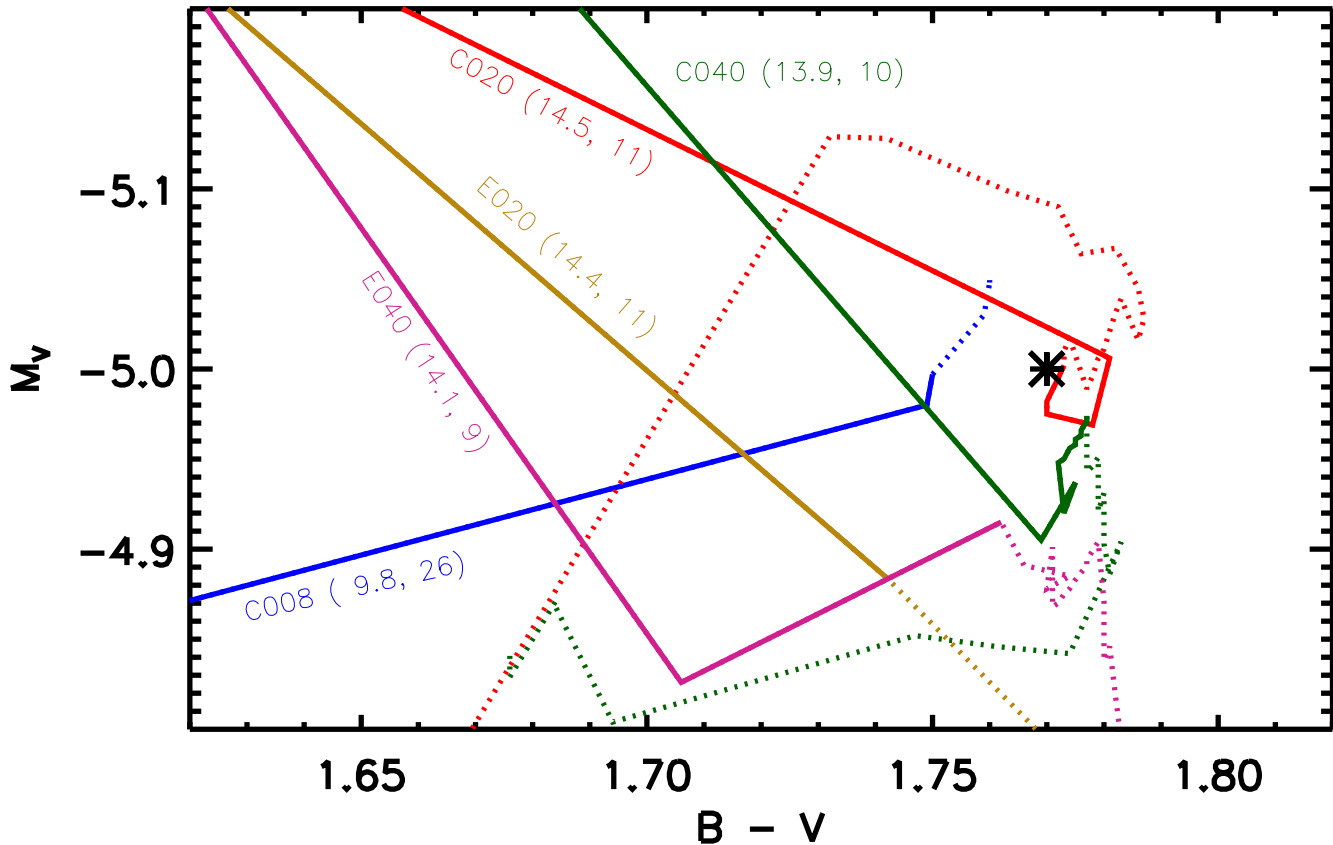


Fig. 1.— Evolutionary state of Betelgeuse. The tracks from the Geneva stellar evolutionary models (Lejeune & Schaerer 2001) are overlaid on a color-magnitude diagram, with the position of Betelgeuse represented by an asterisk. The lines are solid until their closest approach to Betelgeuse in their evolutionary history, after which they are depicted as dotted lines (note that the magnitude range is different for the two axes). The lines are labeled by the model used (the models differ in their masses, mass-loss, and metallicities; see Lejeune & Schaerer for a detailed description). The mass (in M_{\odot}) and age (in Myr) of the star at the point of closest approach is also shown for each model. Inspection of the figure shows that while definitive measurements of the mass and age of Betelgeuse are not feasible due to the large systematic model uncertainties (e.g., masses ranging from 10 to 15 M_{\odot} are plausible) but the majority of the models correspond to a mass of $\approx 14 M_{\odot}$ and an age of ≈ 10 Myr, which we then adopt as the nominal mass and age of Betelgeuse throughout this paper.

2. Data

2.1. *Chandra*

Betelgeuse was periodically observed by *Chandra* from 2001 till 2007 as part of a calibration program to monitor the UV, optical, and IR response of all of the detectors. Of these, we consider the on-axis observations with the ACIS-I, HRC-I, and HRC-S detectors, for which the expected out-of-band contamination is vanishingly small and thus can be ignored (Wolk 2002 for ACIS-I; and Posson-Brown & Kashyap 2005 for HRC, see Table 3). The out-of-band leak is large for the ACIS-S detector, so we do not use any Betelgeuse ACIS-S observations in this analysis. A total of ~ 21 ks of exposure has been accumulated thus far with *Chandra* (see Table 2).

We use level 2 photon event lists downloaded from the public archive, which have gone through the standard pipeline processing by the CXC software (ASCDS versions 6.4 and above). Further analysis was done using CIAO software (v3.2.2) and custom IDL¹ software, including routines from the Package for Interactive Analysis of Line Emission (PINTofALE; Kashyap & Drake 2000).²

For both HRC detectors, we used circular source regions with $r \approx 1''$, enclosing 95% of the X-ray PSF, centered on the location of the source (verified with ACIS-S data, where Betelgeuse is visible due to the optical leak). To measure the background, in the HRC-I we used annuli 30'' wide, beginning 1' away from the source location; for the HRC-S, we used annuli 45'' wide, beginning 35'' away from the source location.

For ACIS-I, we first followed CIAO threads to reprocess the event list from level 1, removing afterglow events and rejecting events with bad grades. We then filtered the new level 2 event list to include PI= 20–170, which corresponds to an energy cut of approximately 0.3 – 2.5 keV. For the source region, we used a circle with $r \approx 3''$, enclosing 99% of the ACIS X-ray PSF, and a background annulus 90'' wide, beginning 10'' away from the source location. To find the combined *Chandra* counts upper limit, we used circular source regions with $r = 10''$ and annular background regions with $r_{min} = 10''$ and $r_{max} = 100''$ for all three detectors (HRC-I, HRC-S, and ACIS-I). The sum of the background counts was used as the background b (see Equation 1 in §3.1) when finding the combined counts upper limit, and the sum of the exposure times was used as the combined exposure time when finding the combined flux upper limit (see §3.2). Observed source and background counts for all

¹Interactive Data Language, ITT Visual Information Solutions

²Available from <http://hea-www.harvard.edu/PINTofALE/>

detectors are listed in Table 4.

2.2. *ROSAT*

Berghöfer et al. (1999) find an X-ray count rate upper limit of 5×10^{-4} ct s⁻¹ for Betelgeuse based on *ROSAT*/HRI observations, and a limit of 10^{-2} ct s⁻¹ based on the *ROSAT* All-Sky Survey data (RASS). For completeness, we have included these estimates in Figure 2, and have also recalculated the limit based on RASS data. Because Betelgeuse is not detected, we estimate the upper limit (see §3) based on the high-resolution X-ray background maps derived from RASS (Snowden et al. 1997). These maps are exposure corrected images with $12' \times 12'$ pixels, in seven energy bands, each with a corresponding error map. We considered bands 1 and 2, spanning 0.11 – 0.284 keV, and bands 1 through 7, spanning 0.11 – 2.04 keV. By averaging the exposure times for eight sources in the RASS Faint Sources Catalog within 1° of Betelgeuse, we estimated the exposure time for the local background to be 460 ± 5 s. To estimate the counts upper limit, we collected background counts within a circle with $r = 35''$ centered on the position of Betelgeuse; such a circle encloses 95% of the PSPC PSF. Observed source and background counts are listed in Table 4. We obtain a limit nearly identical to that derived by Berghöfer et al. for the RASS.

2.3. UV, Optical, and IR Leak

An important concern when optically bright sources are X-ray weak is that counts that may be detected in the instrument could be due to its so called out-of-band response to UV, optical, and IR photons. It is therefore critical to include this leak into estimates of the background. That is, we must compute the X-ray detection limit that includes possible contributions to the observed count rate from lower energy photons.

For the PSPC, we adopt a conservative estimate of $\sim 2 \times 10^{-3}$ ct s⁻¹ for the UV response as quoted in the *ROSAT* User’s Handbook (expected for a high-temperature star such as Vega).³ This implies that only 1 UV photon will be detected during a 460 s exposure. For *Chandra*, an analysis of the out-of-band response of the HRC to Betelgeuse (Posson-Brown & Kashyap 2005) shows that the UV leak from Betelgeuse is vanishingly small (Table 3) and no UV photons will be detected during the HRC observations. A similar estimate also applies to ACIS-I observations (Wolk 2002).

³<http://wave.xray.mpe.mpg.de/rosat/doc/ruh/rosathandbook.html>

3. Analysis

3.1. Counts Upper Limits

To calculate the X-ray counts upper limits, we estimate the counts that would need to be present in order to detect the source above a given background, assuming a Poisson probability distribution for background counts. The probability that at most D counts would be observed as a statistical fluctuation, given a background b , is

$$p(\leq D | b) = \sum_{i=0}^D \frac{b^i e^{-b}}{i!}. \quad (1)$$

The background b is determined locally, from an annulus around the nominal location of the source, and where applicable, an estimate of the UV leak is added to it (see §2). Note that this is a cumulative probability estimate, and uses the full Poisson likelihood in the process. For a specific probability threshold p , the upper limit is $ul(p) = D(p) - b$. We allow for statistical variations in the background counts by doing Monte Carlo simulations where the background counts are sampled from a Poisson distribution. We typically report a “ 3σ ” limit, corresponding to a probability of 0.997 that matches the integrated area under a normalized Gaussian between $\pm 3\sigma$. Note that in our case, for consistency with the Poisson distribution in the low-counts regime, the integration always starts at a counts intensity of 0, and the counts value at which the probability threshold is met does not coincide with the aforementioned $\pm 3\sigma$ range of a Gaussian. For a more detailed description of this approach, see Pease et al. (2006). Our results are summarized in Table 4.

3.2. Flux Upper Limits

The counts upper limit determined above in §3.1 represents the minimum counts that Betelgeuse must have in the source aperture in order to be detected. If it were observed with the same instrumental sensitivity a large number of times, and if it had a true flux intensity that produces, on average, the same number of counts in the source aperture as the quoted counts limit, then it would be detected in half the observations and not detected in the other half. A simple multiplicative transformation of the counts limit to the flux limit can therefore be performed under these conditions by computing a counts-to-energy conversion factor for various putative plasma temperatures.

For each instrument, we generate spectra for isothermal plasma at a given emission measure over a range of temperatures, $T = 0.3 - 10$ MK, using PINTofALE (Kashyap & Drake 2000). We use the CHIANTI database of atomic emissivities (Dere et al. 1997, Young

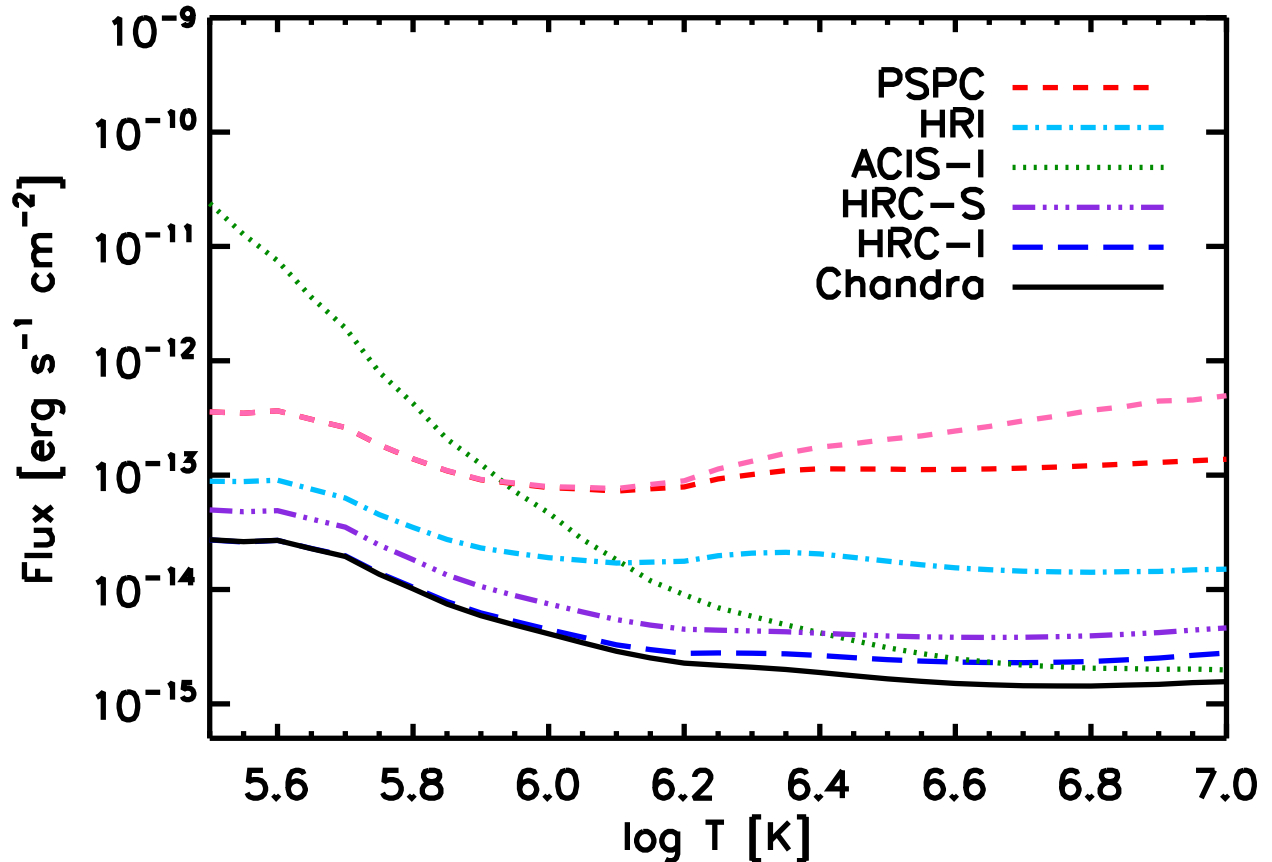


Fig. 2.— Upper limits on the observed X-ray flux from Betelgeuse at Earth, as a function of coronal temperature, based on non-detections from *Chandra* and *ROSAT*. The upper limit curves derived from each of the instruments are shown (PSPC: dashed; we show the results for both the full band [lower curve] and for just the soft band [channels R1 and R2; upper curve]; HRI (from Berghöfer et al. 1999): dot-dashed; ACIS-I: dotted; HRC-S: dash-triple-dotted; HRC-I: long-dashed) as well as the limit from the combined *Chandra* observations (solid line). Note that the *Chandra* limits are significantly below those from *ROSAT*, except for ACIS-I at low temperatures. The combined limit from *Chandra* improves upon previous observations by roughly an order of magnitude.

et al. 2003) with solar abundances (Grevesse et al. 1992) and ion balances from Mazzotta et al. (1998). These spectra, which define the incident intensity at the telescope, are multiplied by the appropriate effective areas and convolved with the instrument response matrices to

obtain the counts predicted in a given passband. The ratio of the incident flux to the derived counts gives a counts-to-flux conversion factor for each temperature, which then allows us to convert the counts upper limits to flux upper limits. These upper limits are shown in Figure 2.

In addition to considering the *Chandra* instruments separately, we also combine them to achieve a more stringent upper limit on Betelgeuse’s X-ray flux. We do this by constructing a virtual observation that is essentially the sum of the individual observations, weighted by the appropriate effective areas and exposure times. For a nominal incident flux from a plasma at a given temperature, we compute the counts predicted for the specific combinations of *Chandra* instruments and exposures in Table 2, and compute the sum of these counts. Because the relative fractions of the counts remain unchanged as the nominal flux changes, the ratio of the summed counts and the input flux gives the counts-to-flux conversion factor for this virtual observation. We thus obtain the most stringent limits on the X-ray flux from Betelgeuse obtained thus far, which ranges from $\approx 2 \times 10^{-14}$ ergs s $^{-1}$ cm $^{-2}$ at $T < 0.5$ MK to as low as 2.2×10^{-15} ergs s $^{-1}$ cm $^{-2}$ at $T = 50$ MK.

The flux limits at Earth can also be converted to intrinsic X-ray luminosity limits at the star after a suitable absorption column density N_H is adopted. The circumstellar shell surrounding Betelgeuse has a column density estimated to be $N_H = 6.2 \times 10^{21}$ cm $^{-2}$ (Hagen 1978), and an additional column of approximately the same magnitude can be present due to chromospheric material that extends above a conjectured “buried corona” (see Ayres et al. 2003). We also consider a smaller value of N_H since part of the circumstellar column is likely to be in dust and grains, which will effectively reduce the absorption column. The ratio L_X/L_{bol} and the corresponding average surface X-ray flux F_X are shown in Figure 3. The implications of the derived upper limits to the surface flux are discussed in §4.2. Throughout this paper, we adopt $L_{\text{bol}} = 1.2 \times 10^{38}$ ergs s $^{-1}$ for Betelgeuse, calculated from the observed visual magnitude.

4. Discussion

4.1. Magnetic Fields

If any coronal plasma exists on the surface of Betelgeuse, it is likely confined in place by magnetic fields. From numerical studies (see §4.2 below), we expect fields of strength approaching 500 G. How does it compare to the observational limit? Here we estimate the magnetic field strength required to confine plasma, assuming that there does exist coronal plasma emitting at a level just below the derived flux upper limit (§3.2), and further assuming

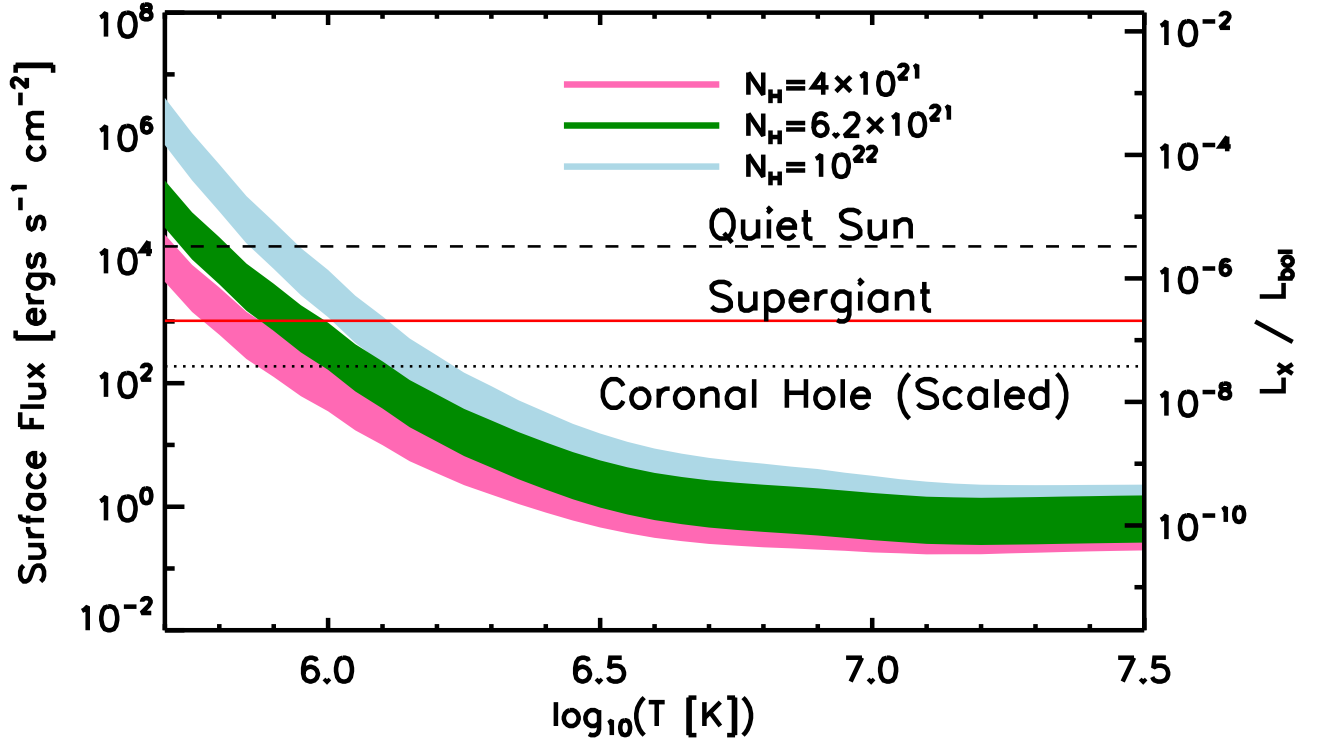


Fig. 3.— Upper limits on the surface X-ray flux, F_X of Betelgeuse as a function of coronal temperature, based on non-detections from *Chandra*. The F_X are calculated for three different values of the column density, one for the nominal column, $N_H = 6.2 \times 10^{21} \text{ cm}^{-2}$ (dark curve in the middle) and the other two representing the uncertainty in our choice of N_H (light curves), at $N_H = 4 \times 10^{21}$ (lower curve) and 10^{22} cm^{-2} (upper curve). The width of the shaded regions represent the measurement errors in the distance and diameter of Betelgeuse, as well as the statistical uncertainty in the precision with which the counts upper limit is determined. The horizontal lines represent the surface flux of the quiet Sun (dashed), the same flux scaled to match the magnetic field strength on Betelgeuse (solid), and the flux from solar coronal holes scaled to match Betelgeuse (dotted); this is discussed in §4.2. The scale along the right represents the L_X/L_{bol} values corresponding to the nominal distance and size of Betelgeuse.

equipartition of thermal and magnetic energy densities in the corona, i.e., $\frac{B^2}{8\pi} = 2n_e k_B T$, and hence

$$B = \left(\frac{16\pi\mu^2 k_B^2 T^2 L_X}{hR_*^2 f\Lambda(T)} \right)^{1/4} \quad (2)$$

where T is the assumed plasma temperature, $\Lambda(T)$ is the power emitted from a unit volume of the plasma, μ is the effective mass of an average particle ($\mu \approx \frac{1}{2}$ for fully ionized plasma), R_* is the stellar radius, k_B is Boltzmann’s constant, f is the filling fraction of the X-ray active region on the surface of the star, and h is the height of the corona. Note that $B \propto (L_X/f)^{1/4}$, i.e., it is only weakly dependent on the X-ray luminosity and the filling fraction.

In Figure 4, we show the required field strength B , for a range of filling fraction f , for different estimates of the height of the corona. We obtain estimates both for a corona that is approximately the same height as the solar corona ($h = 10^{10}$ cm) and for one that extends as high as the chromospheric scale height ($h = kT_{\text{chrom}}R_*^2/\mu m_H GM_* \approx 2 \times 10^{12}$ cm). The latter is relevant in the context of a “buried corona” scenario expounded by Ayres et al. (2003). We find that the required B ranges from $\lesssim 0.1$ G up to ≈ 5 G, considerably less than the field strength expected from modeling (Dorch 2004). Weaker fields are sufficient for lower levels of X-ray emission. (Note that our calculation of B is not a limit, and we cannot rule out the presence of a stronger magnetic field. However, we can say that a stronger magnetic field is *not required*.) We thus conclude that sustaining a weak corona on Betelgeuse is feasible, and such coronae cannot yet be ruled out based on the X-ray flux limits.

4.2. Magnetic Carpet

Numerical MHD simulations of stars such as Betelgeuse have shown that a highly structured magnetic dynamo may operate on them (Dorch 2004, Freytag et al. 2002), with field strength as high as $B_* \approx 500$ G. The energy spectra of the magnetic energy density peaks cascade to small scales, with a preponderately high contribution at scales $\sim \frac{1}{10}R_*$. This is very similar to the magnetic activity in the quiet Sun, where for comparison, field strengths reach up to ~ 2000 G (Cerdeña et al. 2006), and the magnetic structures of mixed polarity emerge uniformly over the surface on timescales approximately the same as the convective cells. This is the so-called ‘magnetic carpet’ (Schrijver et al. 1997, Title 2000) which pervades the surface of the Sun away from active regions.

If red supergiants are magnetically active in a similar manner, the total energy dumped into the corona, and the resulting plasma temperatures and X-ray luminosities, are similar in scope to that seen in the quiet Sun and in coronal holes, scaled only by the energy densities and volumes involved. We assess the feasibility of this scenario by computing the expected surface flux upper limit F_X for Betelgeuse. Figure 3 shows bands corresponding to the surface flux limits, calculated assuming a variety of plausible absorbing column densities, $N_H = (4, 6.2, 10) \times 10^{21}$ cm⁻² (see §3.2). Here we assume that the entire surface is covered by magnetic structures that contribute to the X-ray emission, i.e., that the filling fraction

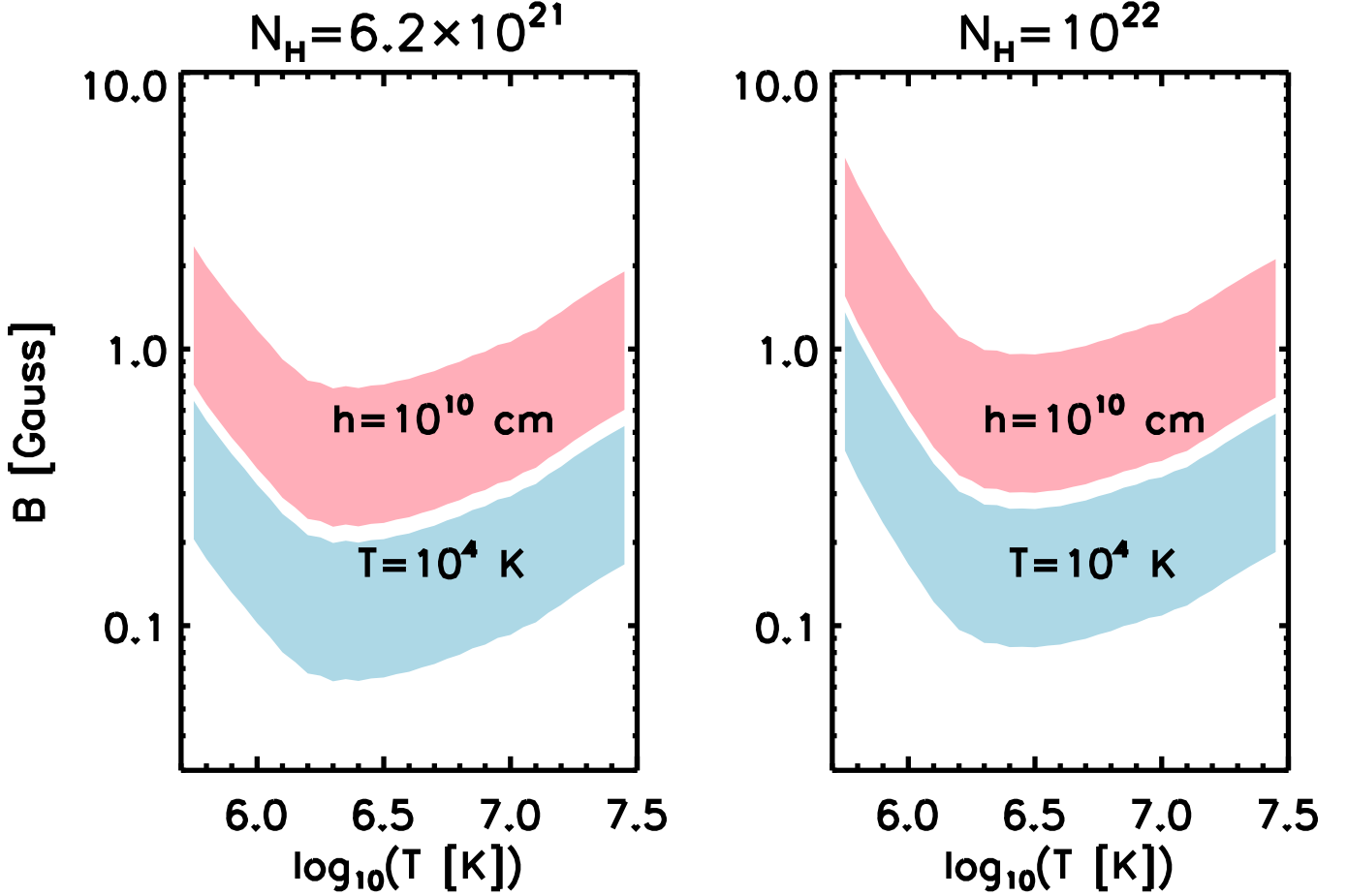


Fig. 4.— Magnetic field strength B required to confine coronal plasma on Betelgeuse, as a function of the plasma temperature. The shaded regions represent the variation expected due to a patchy coverage of the surface by the magnetic field, with the lower edges corresponding to a filling fraction $f = 1$ and the upper edges to $f = 0.01$. The lower shaded regions represent a corona with the same height as the scale height of the chromosphere, and for comparison, the upper shaded regions represent a corona with a similar height as that of the solar corona. The two plots are calculated assuming different column densities of absorption: $N_H = 6.2 \times 10^{21}$ (left) and 10^{22} cm^{-2} (right).

$f = 1$. However, supergiant stars like Betelgeuse possess very large convection cells (Lim et al. 1998) which suggests that $f \ll 1$. Smaller values of f imply that the surface flux upper limit will be correspondingly higher. We show the effects of smaller filling fractions in Figure 4.

The X-ray luminosity of the quiet Sun is $\approx 10^{27}$ ergs s $^{-1}$ (Golub & Pasachoff 1997) corresponding to a surface flux of 1.64×10^4 ergs s $^{-1}$ cm $^{-2}$. If similar processes to those on the Sun operate on Betelgeuse, it is reasonable to expect that the energy flux deposited into the corona will be similar, scaled by the available magnetic energy density. Thus, we expect a surface X-ray flux of $\approx 10^3$ ergs s $^{-1}$ cm $^{-2}$ on Betelgeuse. Note however that the surface flux on Betelgeuse could be lower if it were dominated by features similar to the solar coronal holes. The X-ray flux from coronal holes on the Sun is much lower, $\approx 3 \times 10^3$ ergs s $^{-1}$ cm $^{-2}$ (Vernazza & Smith 1977, Schrijver et al., 2004), and again scaling it to the expected magnetic field energy density present on Betelgeuse, we obtain a possible X-ray surface flux of ≈ 200 ergs s $^{-1}$ cm $^{-2}$ (see Figure 3).

The upper limit on F_X is strongly dependent on the temperature of the plasma because of the sensitive dependence of the observable spectrum on the absorption column. We find that the limit is as low as 1 ergs s $^{-1}$ cm $^{-2}$ ($L_X/L_{\text{bol}} \approx 10^{-10}$) at high temperatures, but cannot be reduced below $\approx 10^2 - 10^3$ ergs s $^{-1}$ cm $^{-2}$ for $T < 1$ MK ($L_X/L_{\text{bol}} \approx 10^{-8} - 10^{-7}$) for the sensitivity achieved thus far with *Chandra*. While the upper limit at low temperatures still lies above the flux expected from the solar analogy, this calculation does rule out the existence of pervasive quiet Sun type emission at high temperatures, since a surface flux of $\approx 10^2 - 10^3$ ergs s $^{-1}$ cm $^{-2}$ from plasma at $T > 2$ MK would have been easily detected. Note however that this does not preclude patchy and highly localized regions of magnetic activity that produces high temperature plasma, or more pervasive low-temperature plasma emission arising from this mechanism: plasma at $T \lesssim 1$ MK will remain undetected at the sensitivity limit of our observations. Since the quiet Sun and coronal hole plasma is at $T \gtrsim 1$ MK, this further suggests that even if hot plasma at lower temperatures is present on Betelgeuse, it will bear little resemblance to the solar case.

4.3. Coronal Proxies

Numerous UV and FUV chromospheric lines have been identified as proxies for coronal activity in normal and giant stars. Note that the physical relationship between the mechanisms that generate coronal and chromospheric line emission is poorly understood, and the proxy lines are often formed at temperatures very different from those that characterize coronae. However, assuming that similar processes occur on Betelgeuse as on coronally active giants and main sequence stars, we investigate whether our derived flux upper limits (see §3.2) are consistent with observations of coronal proxy lines on Betelgeuse. Based on known correlations between X-ray flux and proxy lines such as CIV, SiIV, etc., we can estimate the X-ray luminosity that can be expected from Betelgeuse.

For main sequence stars, Redfield et al. (2003) find a strong correlation between the soft X-ray flux and the Fe XVIII $\lambda 974$ flux (see their Figure 7) from *FUSE* (Far Ultraviolet Spectroscopic Explorer) spectra of main sequence and late-type stars. Fe XVIII forms above $T = 2$ MK, and has a peak response at $T = 6$ MK, and is thus sensitive to plasma temperatures similar to that on active binaries such as Capella. Redfield et al. place an upper limit of 8×10^{-13} ergs s $^{-1}$ cm $^{-2}$ on the Fe XVIII flux from Betelgeuse ($L_{\text{FeXVIII}}/L_{\text{bol}} = 7.5 \times 10^{-11}$) which implies a value for the unabsorbed X-ray luminosity $L_X/L_{\text{bol}} < 10^{-7}$ if supergiants such as Betelgeuse follow the correlation seen in their Figure 7. The flux upper limit we calculate (§3.2, Figure 3) corresponds to $L_X/L_{\text{bol}} < 10^{-9}$ for $T > 1$ MK, well below the value predicted by the main sequence correlation. Conversely, assuming that the correlation is valid for supergiants, our X-ray upper limit implies a stronger constraint on the Fe XVIII emission, $L_{\text{FeXVIII}} < 7.5 \times 10^{-13} L_{\text{bol}}$.

Similarly, there exists a clear correlation between CIV and X-ray luminosities for giant stars (see, e.g., Ayres et al. 1997, especially their Figure 2). Even though there is evidence for considerable scatter for different types of stars, one can establish a general correspondence that is valid to within an order of magnitude. Based on *IUE* ultraviolet spectra, Basri et al. (1981) place a 3σ upper limit of 1.5×10^{-13} ergs s $^{-1}$ cm $^{-2}$ on the CIV $\lambda 1549$ flux from Betelgeuse, and this translates to an unabsorbed X-ray luminosity limit of $L_X/L_{\text{bol}} \lesssim 10^{-9}$. In the temperature range $T = 1 - 10$ MK (which matches the sensitivity range of X-ray measurements from *Einstein* and *ROSAT*, on which this correlation is based), this limit is comparable to our observational limit determined above.

Lastly, from *FUSE* spectra of Betelgeuse published by Dupree et al. (2005; see their Figure 4), we estimate an upper limit of 3×10^{-14} ergs s $^{-1}$ cm $^{-2}$ on its Si IV flux. If the correlation found by Ayres et al. (2003, see their Figure 4) for giant stars applies to supergiants like Betelgeuse, then the limit of $f_{\text{SiIV}}/f_{\text{bol}} < 5 \times 10^{-10}$ corresponds to an expected X-ray unabsorbed flux of $f_X/f_{\text{bol}} \lesssim 10^{-9}$ which is again comparable to the observed limit we obtain.

Note that previous studies of Betelgeuse in the optical and UV have seen no evidence for chromospheric temperatures above 6000 K (e.g. Lobel et al. 2000 & 2001 and Carpenter et al. 1994) and our observations are consistent with those findings.

From the comparisons above, we conclude that we have now achieved a sensitivity in the X-ray regime that is comparable to the sensitivity achieved in the far UV with coronal proxy lines, especially at temperatures $T > 3$ MK. In combination with the surface flux limit arguments made above (§4.2) and the stringent upper limit on L_X/L_{bol} obtained here, we conclude that any high-temperature plasma will have to arise from a mechanism other than that which normally operates on the Sun.

Finally, note also that if the hot plasma is “buried” in the highly extended chromospheric material (as suggested by Ayres et al. 2003), then both the chromospheric proxies and the coronal X-ray flux will be subject to significant absorption, and our placement of Betelgeuse on these flux-flux correlation diagrams will be systematically low. In such a case, the limit on L_X/L_{bol} will be less restrictive, but will not affect our conclusions.

5. Summary

We have carefully analyzed over 20 ks of *Chandra* observations of Betelgeuse in an effort to detect X-ray emission from the massive red supergiant. However, Betelgeuse remains undetected, and we derive an upper limit to the X-ray count rate by calculating the rate that would have resulted in a detection given the extant background. We have converted this count rate limit to a flux limit at the telescope by computing the response of *ROSAT* and *Chandra* instruments to isothermal plasma producing optically-thin thermal emission, and thereby derive the most stringent upper limits to the X-ray flux from Betelgeuse obtained thus far. We find a limit for the flux from Betelgeuse at the telescope of $f_X < 4 \times 10^{-15}$ ergs s⁻¹ cm⁻² for temperatures $T > 1$ MK. At lower temperatures, we place a limit of $f_X < 3 \times 10^{-14}$ ergs s⁻¹ cm⁻² on the flux.

The flux limit at Earth can be converted to a stellar surface flux upper limit and to an L_X/L_{bol} limit using the known distance and size of Betelgeuse. We compare the surface flux limits with the flux expected from a solar like emission mechanism, where a pervasive magnetic field maintains a low-level corona, as in the quiet Sun or solar coronal holes. We rule out such emission at temperatures > 1 MK, but such emission is still feasible at lower temperatures. The minimum magnetic field necessary to maintain such a corona is < 10 G, well within theoretical expectations.

We compare the L_X/L_{bol} upper limit we derive with the limits obtained from non-detections of coronal tracer lines such as CIV, SiIV, and FeXVIII $\lambda 974$ and find that we achieve sensitivities in the X-ray comparable to that in the coronal proxies. These limits reinforce the conclusions arrived at above, that high-temperature plasma, even at levels expected in the presence of stellar coronal holes, is absent on Betelgeuse, but the existence of low-temperature plasma cannot be ruled out.

JPB, VLK, DOP, and JJD were supported by NASA contract NAS8-39073 to the *Chandra X-ray Center* during the course of this research. We thank Tom Ayres for useful feedback on determining upper limits. VLK thanks Andreas Zezas, Steve Saar, and Mark Weber for useful discussions. This research has made use of the SIMBAD database, operated at CDS,

Strasbourg, France.

REFERENCES

- Ayres, T.R., Brown, A., & Harper, G.M. 2003, ApJ, 598, 610
- Ayres, T.R., et al. 1997, ApJ, 491, 876
- Basri, G.S. Linsky, J.L., & Eriksson, K. 1981, ApJ, 251, 162
- Berghöfer, T.W., Schmitt, J.H.M.M., & Hünsch, M., 1999, A&A, 342, L17
- Burns, D., Baldwin, J. E., Boysen, R. C., Haniff, C. A., Lawson, P. R., Mackay, C. D., Rogers, J., Scott, T. R., Warner, P. J., Wilson, D. M. A., Young, J. S., 1997, MNRAS, 290, 11
- Carpenter, K.G., Robinson, R.D., Wahlgren, G.M., Linsky, J.L., & Brown, A., 1994, ApJ, 428, 329
- Cerdeña, I.D., Almeida, J.S., & Kneer, F., 2006, ApJ, 636, 496
- Dere, K.P., Landi, E., Mason, H.E., Monsignori Fossi, B.C., Young, P.R. 1997, A&AS, 125, 149
- Dorch, S.B.F. 2004, A&A, 423, 1101
- Dupree, A.K., Lobel, A., & Young P.R. 2005, ApJ, 622, 629
- Freytag, B., Steffen, M., & Dorch, B., 2002, AN, 323, 213
- Golub, L., & Pasachoff, J.M., 1997, *The Solar Corona*, Cambridge University Press
- Gray, D.F. 2000, ApJ, 532, 487
- Grevesse, N., Noels, A., & Sauval, A.J. 1992, in *Coronal Streamers, Coronal Loops and Coronal and Solar Wind Composition*, Proc. 1st SOHO Workshop, ESA SP-348, ESA Publ. Div., ESTEC, Noordwijk, p.305
- Hünsch, M., Schmitt, J.H.M.M., Schröder, K.-P., & Zickgraf, F.-J., 1998, A&A, 330, 225
- Hünsch, M., & Schröder, K.-P., 1996, A&A, 309, L51
- Hagen, W., 1978, ApJS, 38, 1
- Haisch, B.M., Schmitt, J.H.M.M., & Rosso, C., 1991, ApJ, 383, L15
- Harper, G.M., Brown, A., & Lim, J., 2001, ApJ, 551, 1073
- Kashyap, V. & Drake, J. J. 2000, Bull.Astr.Soc. of India, 28, 475
- Lambert, D.L., Brown, J.A., Hinkle, K.H., Johnson, H.R., 1984, ApJ, 284, 223

- Lesh, J.R., 1968, *ApJ*, 152, 905
- Levesque, E.M., Massey, P., Olsen, K.A.G., Plez, B., Josselin, E., Maeeder, A., Meynet, G., 2005, *ApJ*, 628, 973
- Lim, J., Carilli, C.L., White, S.M., Beasley, A.J., & Marson, R.G. 1998, *Nature*, 392, L575
- Lobel, A. & Dupree, A.K., 2000, *ApJ*, 545, 454
- Lobel, A. & Dupree, A.K., 2001, *ApJ*, 558, 815
- Mazzotta, P., Mazzitelli, G., Colafrancesco, S., & Vittorio, N., 1998, *AASS*, 133, 403
- Pease, D.O., Drake, J.J., & Kashyap, V.L., 2006, *ApJ*, 636, 426
- Perryman, M.A.C., et al., 1997, *A&A*, 323, L49
- Posson-Brown, J. & Kashyap, V. 2005, 2005 Chandra Calibration Workshop
http://cxc.harvard.edu/ccw/proceedings/05_proc/index.html
- Posson-Brown, J., Kashyap, V.L., Drake, J.J., & Pease, D.P., 2005, at Six Years of *Chandra* Symposium
- Redfield, S., et al. 2003, *ApJ*, 585, 993
- Richichi, A., & Percheron, I., 2002, *A&A*, 386, 492
- Rosner, R., Musielak, Z.E., Cattaneo, F., Moore, R.L., & Suess, S.T., 1995, *ApJ*, 442, 25
- Schrijver, C.J., Sandman, A.W., Aschwanden, M.J., & DeRosa, M.L., 2004, *ApJ*, 615, 512
- Schrijver, C.J., Title, A.M., van Ballegooijen, A.A., Hagenaar, H.J., & Shine, R.A., 1997, *ApJ*, 487, 424
- Simon, T., Linsky, J.L., & Stencel, R.L., 1982, *ApJ*, 257, 225
- Snowden, S. L., Egger, R., Freyberg, M. J., McCammon, D., Plucinsky, P. P., Sanders, W. T., Schmitt, J. H. M. M., Trümper, J., Voges, W., 1997, *ApJ*, 485, 125
- Title, A.M., 2000, *Phil.Trans.R.Soc.Lond.A*, 358, 657
- Vernazza, J.E., & Reeves, E.M., 1978, *ApJS*, 37, 485
- Wilson, R. W., Dhillon, V. S., & Haniff, C. A., 1997, *MNRAS*, 291, 819
- Wolk, S. 2002, 2002 Chandra Calibration Workshop
http://cxc.harvard.edu/ccw/proceedings/02_proc/index.html
- Young, P.R., del Zanna, G., Landi, E., Dere, K.P., Mason, H.E., & Landini, M., 2003, *ApJS*, 144, 135

Table 1. Stellar parameters for Betelgeuse

Other Names	α Ori / 58 Ori / HD 39801 / HR 2061 / SAO 113271 / HIP 27989	
(R.A., Dec)	(05:55:10.3053, +07:24:25.426)	ICRS 2000.0
($l_{\text{II}}, b_{\text{II}}$)	(199°.79, $-8^\circ.96$)	SIMBAD
Spectral Type	M2 Iab	SIMBAD
m_V	$0^m.58$	SIMBAD
$B - V$	$1^m.77$	SIMBAD
T_{eff}	3650 K	Levesque et al. (2005)
$B.C.$	-1.6	Levesque et al. (2005)
Distance	131 ± 28 pc	Hipparcos (Perryman et al. 1997)
L_{bol}	1.2×10^{38} ergs s^{-1}	
Angular Diameter	44.6 ± 0.2 mas	CHARM (Richichi & Percheron 2002)
Radius	$631 \pm 134 R_{\odot}$	
Mass	$14 M_{\odot}$	Figure 1
Age	10 Myr	Figure 1
Gravity	$1 \pm 0.4 \text{ cm s}^{-2}$	
Circumstellar Column	$6.2 \times 10^{21} \text{ cm}^{-2}$	Hagen (1978)

Table 2. X-ray Observations of Betelgeuse

Obs ID	Instrument	Date	Exposure (s)
RASS	<i>ROSAT</i> /PSPC, bands 1-7	1990-07-30 ^a	460 ^b
RASS	<i>ROSAT</i> /PSPC, bands 1-2	1990-07-30 ^a	460 ^b
3365	<i>Chandra</i> /ACIS-I	2001-12-16	4897.2
2595	<i>Chandra</i> /HRC-I	2001-12-07	1892.1
3680	<i>Chandra</i> /HRC-I	2003-02-06	1893.4
5055	<i>Chandra</i> /HRC-I	2004-02-02	2075.9
5970	<i>Chandra</i> /HRC-I	2005-02-02	2129.4
2596	<i>Chandra</i> /HRC-S	2001-12-07	1926.7
3681	<i>Chandra</i> /HRC-S	2003-02-06	1819.6
5056	<i>Chandra</i> /HRC-S	2004-02-02	1945.3
5971	<i>Chandra</i> /HRC-S	2005-02-02	2140.4

^aStart date of RASS

^bEstimated from nearby sources (see §2)

Table 3. UV leak upper limits for HRC observations of Betelgeuse at the aimpoint. The predicted count rates (and 1σ bounds) based on the UV/optical flux of Betelgeuse are compared with the upper limits derived from the accumulated data. The time required for a detection at 99.7% significance, derived from comparison of the predicted rate to the upper limit, is also noted. (Posson-Brown & Kashyap 2005)

Detector	Expected count rate [ct s ⁻¹]	Accumulated Exposure [s]	Upper Limit [ct s ⁻¹]	Required Exposure
HRC-I	$1.29^{+0.11}_{-0.14} \times 10^{-6}$	7991	7.04×10^{-4}	$\sim 2 \times 10^9$ s
HRC-S	$1.64^{+0.86}_{-0.71} \times 10^{-5}$	7832	1.86×10^{-3}	$\sim 9 \times 10^7$ s

Table 4. 3σ Counts Upper Limits on Betelgeuse

Detector	Exposure	Background Region		Source Region		Upper Limit
	t_{exp} [s]	a_{bkg} [arcsec ²]	N_{bkg} [ct]	a_{src} [arcsec ²]	N_{src} [ct]	$D - b$ [ct]
<i>ROSAT</i> /PSPC bands 1-2	460	4147200	234	3848	38	6
<i>ROSAT</i> /PSPC bands 1-7	460	4147200	358	3848	48	6
<i>Chandra</i> /HRC-I	7791	14126	1052	2.66	0	2
<i>Chandra</i> /HRC-S	7832	16245	9340	2.66	4	4
<i>Chandra</i> /ACIS-I	4897	31102	50	28.27	0	2
<i>Chandra</i> combined ^a	20720	31102	20384	28.27	19	13

^aNote that the size of the source region used when finding the combined limit is larger than the source sizes used when finding the HRC limits (see §2.1)